



# Kent Academic Repository

Matshaba, Malili G., Sayle, Dean C., Sayle, Thi X. T. and Ngoepe, Phuti Esrom (2016) *The Structure of Surface Entrance Sites for Li-intercalation into TiO<sub>2</sub>Nanopar Nanosheets and Mesoporous Architectures with Application for Li-ion Batteries.* *Journal of Physical Chemistry C*, 120 (26). pp. 14001-14008. ISSN 1932-7447.

## Downloaded from

<https://kar.kent.ac.uk/55850/> The University of Kent's Academic Repository KAR

## The version of record is available from

<https://doi.org/10.1021/acs.jpcc.6b04770>

## This document version

Author's Accepted Manuscript

## DOI for this version

## Licence for this version

UNSPECIFIED

## Additional information

## Versions of research works

### Versions of Record

If this version is the version of record, it is the same as the published version available on the publisher's web site. Cite as the published version.

### Author Accepted Manuscripts

If this document is identified as the Author Accepted Manuscript it is the version after peer review but before type setting, copy editing or publisher branding. Cite as Surname, Initial. (Year) 'Title of article'. To be published in *Title of Journal*, Volume and issue numbers [peer-reviewed accepted version]. Available at: DOI or URL (Accessed: date).

## Enquiries

If you have questions about this document contact [ResearchSupport@kent.ac.uk](mailto:ResearchSupport@kent.ac.uk). Please include the URL of the record in KAR. If you believe that your, or a third party's rights have been compromised through this document please see our [Take Down policy](https://www.kent.ac.uk/guides/kar-the-kent-academic-repository#policies) (available from <https://www.kent.ac.uk/guides/kar-the-kent-academic-repository#policies>).

# The Structure of Surface Entrance Sites for Li-intercalation into TiO<sub>2</sub> Nanoparticles, Nanosheets and Mesoporous Architectures with Application for Li-ion Batteries

Malili G. Matshaba<sup>1</sup>, Dean C. Sayle<sup>2</sup>, Thi X. T. Sayle<sup>1, 2</sup> and Phuti E. Ngoepe<sup>\*1</sup>,

<sup>1</sup> Materials Modeling Center, University of Limpopo, Private Bag x1106, Sovenga, 0727, South Africa.

<sup>2</sup> School of Physical Sciences, University of Kent, Canterbury, Kent, CT2 7NZ, United Kingdom.

## ABSTRACT

Power output is central to the viability of a Li-ion battery, and is, in part, dependent upon the activation energy barrier associated with Li intercalation/deintercalation into the host lattice (electrode). The lower the energy barrier, the faster the intercalation reaction rate and greater the power. The activation energy is governed by the atomistic structure(s) of the entrance sites for Li intercalation. Accordingly, a first step in optimising battery power via structural manipulation of entrance sites, is to understand the structure of these entrance sites. However, HRTEM is (presently) unable to characterise the structures of entrance sites with atomistic resolution. Accordingly, we generate models of the entrance sites using Molecular Dynamics. In particular, we simulate the synthetic protocol used to fabricate nanostructured TiO<sub>2</sub> experimentally. The resulting atomistic models reveal a highly complex and diverse structural distribution of entrance sites, which emanate from the surface curvature of the nanostructured material. In particular, we show how nanostructuring can be used to change profoundly the nature and concentration of such entrance sites.

## INTRODUCTION

Nanostructured materials have shown great promise recently as potential electrodes for Li-ion batteries [1,2]. In particular, Ren et al. showed that mesoporous TiO<sub>2</sub>, with a 3D pore structure, can be used as an anode replacing graphite.[3] Similarly, mesoporous MnO<sub>2</sub> can act as a cathode [4]. Nanostructuring of the electrodes was shown, in both cases, to confer electrochemical activity upon the materials [5]; the parent bulk materials are electrochemically inactive. A recent simulation study revealed that mesoporous materials are able to expand and contract elastically (during charge cycling) as pseudo ‘breathing-crystals’ – enabling retention of the structure and crucially the 1x1 tunnels in which the Li ions enter and reside [6]. Conversely, the bulk parent material deforms plastically during intercalation pulverising the tunnels [4,6].

Central to the power output and charge time of batteries is the activation energy barriers associated with Li intercalation/deintercalation from the host electrodes. The lower the energy barriers, the faster the reactions facilitating higher power and lower charge times. The activation energy is governed by the atomistic structure(s) of the entrance sites for Li intercalation. Accordingly, a first step in tuning battery power, via structural manipulation of entrance sites, is to understand their structure.

Inspection of HRTEM images of mesoporous TiO<sub>2</sub>, fig 1, reveals that the entrance sites are not structurally uniform [3]; rather the figure reveals a diverse structural complexity, which emanates from the three-dimensional curvature of the pore. Accordingly, if one were to use a model of the perfect surface to calculate energy barriers associated with Li intercalation, the results would prove erroneous because the model would not capture the structural perturbations emanating from the curvature of the surface. Indeed, Tompsett and co-workers showed that structure has a profound impact upon the energy barriers for Li intercalation [7]. In particular, notwithstanding the curvature of a nanostructured system, the group used Density Functional Theory (DFT) to show that the energy barrier associated with Li intercalation into  $\beta$ -MnO<sub>2</sub> (isostructural with rutile, TiO<sub>2</sub>) can change from 0.6eV to less than 0.3eV for the (101) and (001) surfaces of  $\beta$ -MnO<sub>2</sub> respectively.[7] Accordingly, if reliable predictions, pertaining to activation energy barriers for Li intercalation into nano-structured TiO<sub>2</sub>, are to be proffered by simulation, the model must capture the structural complexity of the curved pore surface.

HRTEM is (presently) unable to characterise the structures of entrance sites with atomistic resolution, fig 1; rather only the interconnecting networks of pores, fig 1(a) [8] and interatomic planes, fig 1(b), [3] at the pore surfaces are evident from HRTEM. What is missing, are three dimensional atomistic structures of the entrance sites, from which one can (visually) understand how Li may intercalate into the host lattice. Accordingly, in this study, we use MD simulation to generate atomistic models of the surface entrance sites.

Normally, atomistic models are generated by utilising experimental data, such as atom positions derived from XRD or HRTEM, but this is not possible at present because the structural complexity of a mesoporous material is such that such the atom positions cannot (yet) be extracted from experiment. An alternative approach is to use chemical intuition coupled with symmetry operators. However, this approach also becomes intractably difficult when one considers that the unit cell of a mesoporous material comprises tens of thousands of atoms. Moreover, the model must also capture microstructural features such as dislocations and grain-boundaries and the morphologies of the (internal) pore surfaces, which will influence Li intercalation.

Hierarchical structural complexity of nanostructured materials, which includes the polymorphic crystal structure, microstructure and nanostructure<sup>i</sup>, emanates ultimately from the synthetic protocol used in their experimental fabrication. Accordingly, the approach we use in this study, to generate atomistic models that are realistic, in that they capture the hierarchical structural complexity, is to simulate the synthetic protocol. Specifically, we simulate the crystallisation of the nanostructured material starting from amorphous precursors. The size of the unit cell,

---

<sup>i</sup> Microstructure includes, for example: dislocations, grain-boundaries, intrinsic point defects; nanostructure includes: architecture of pore network, curvature of (internal) surfaces.

required to capture such structural complexity, is of the order of tens of thousands of atoms, and therefore ab-initio methods are presently computationally prohibitive. Consequently, we use atomistic simulation to generate the structural models.

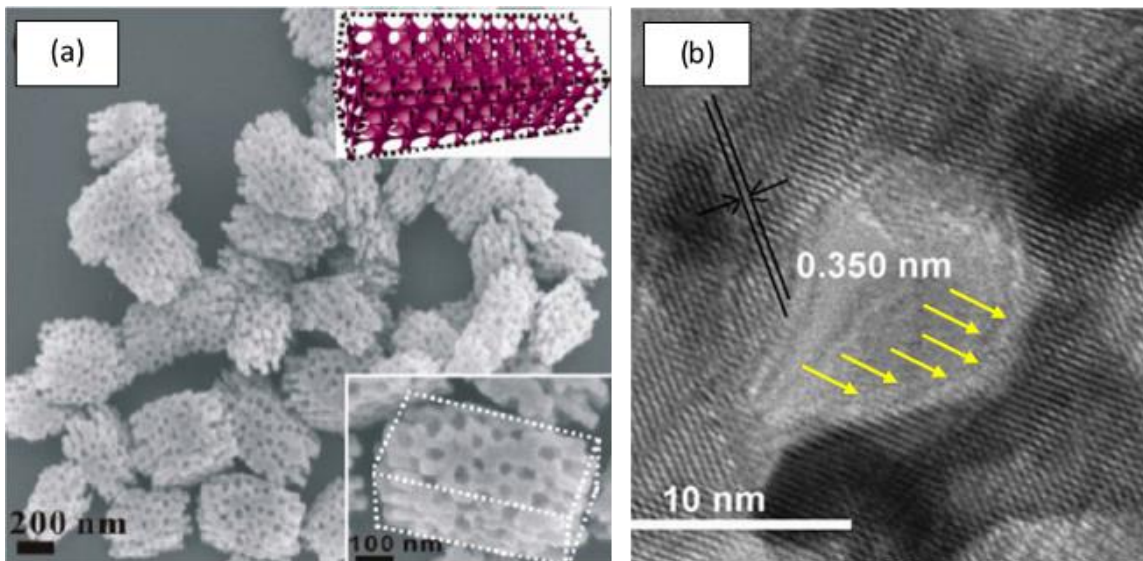


**Figure 1.** HRTEM of mesoporous  $\text{TiO}_2$  (a) Mesoporous rutile-structured  $\text{TiO}_2$ , reproduced with permission from ref [8]. Copyright American Chemical Society 2013 (b) Anatase  $\text{TiO}_2$  reproduced with permission from ref [3]; the yellow arrows indicate the positions of possible entrance sites revealing the difficulty in characterising the entrance sites for Li intercalation. Copyright American Chemical Society 2010.

## METHODS

### Potential models and simulation code

All calculations presented in this study are based on the Born model of ionic solids, where titanium (Ti) and oxygen (O) ions interact via long-range Coulombic interactions and short-range parameterised interactions of the Buckingham form. The potentials used in this study were optimized by Matsui [9] and are able to reproduce the four polymorphs of  $\text{TiO}_2$  (rutile, anatase, brookite and  $\text{TiO}_2(\text{II})$ , which is isostructural with  $\alpha\text{-PbO}_2$ ). The parameters are reported in table S1 and S2 (supporting information).

One of the most rigorous tests of a potential model is its ability to simulate crystallisation. In particular, the potential must describe interatomic distances far from the equilibrium distance and capture the amorphous-to-crystalline state (following both the kinetics and thermodynamics associated with the combination of ‘random’ atom collisions that together manifest in the evolution of a nucleating seed). Moreover, the simulation must capture the *spontaneous* evolution of the seed, which nucleates crystallisation of the polymorphic crystal structures. The potential model we have chosen is able to successfully simulate crystallisation of nanotitania to yield the polymorphic crystal structures (rutile and brookite) in accord with experiment [10] and therefore we argue that the potential model we have chosen is appropriate to accurately represent the material.

All the molecular dynamical simulations were performed using the computer code DL\_Poly [11]. The user manual provides comprehensive analytical descriptions and discussion of the molecular dynamics simulations, force fields, boundary conditions, algorithms and parallelization methods used in these simulations.

### **Generating Atomistic models**

During experimental synthesis, mesoporous TiO<sub>2</sub> emanates from an amorphous pre-cursor and then undergoes crystallisation into the mesoporous nanoform [8]. We simulate directly this process. In particular, we start with amorphous precursors and allow the system to crystallise under MD simulation. Analogous to experiment, we control only the temperature of the system: At a particular instant in time, under MD simulation, the combination of atom collisions spontaneously results in the evolution of a crystalline seed. This seed then nucleates crystallisation to facilitate the polymorphic crystal structures (rutile and brookite), the microstructure (dislocations and grain-boundaries) and nanostructure (network of interconnecting pores, and curved (internal) surface morphologies) in accord with experiment.

We argue that because our procedure of ‘simulating synthesis’ generates models with three levels of hierarchical structural complexity (crystal structure, microstructure, nanostructure) in accord with experiment, starting from an amorphous starting point, by just controlling the simulation temperature, our methodological approach is valid. We now describe in detail how each nanostructural model was generated.

**Amorphous Precursor** The atomistic models for the nanoparticle, nanosheet, nanoporous architecture and bulk material were generated using a molten TiO<sub>2</sub> nanoparticle precursor. In particular, a particle of TiO<sub>2</sub> comprising 15972 atoms (5324 titanium and 10648 oxygen atoms), was cut from the parent bulk material. The nanoparticle was then melted by heating to 6000 K, which is above the melting point for TiO<sub>2</sub>, under MD simulation. The molten nanoparticle was then used as the ‘building-block’ to generate the nanoparticle, nanosheet, nanoporous architectures and bulk material.

**Nanoparticle.** Here, the molten TiO<sub>2</sub> nanoparticle was placed in a simulation cell with dimensions sufficiently large that the nanoparticle does not interact with its images. NVT simulation was then performed at 2000 K for 3.5 ns to facilitate crystallisation of the nanoparticle. 20 GPa pressure was imposed upon the nanoparticle to facilitate crystallisation, which was communicated via a pseudo-gas following the procedure in ref.[10]. The low-temperature structural model was then generated by removing the pressure and cooling the system to 0 K under NVT MD simulation, which acts effectively as a pseudo energy minimisation.

**Nanosheet** For the nanosheet, a cubic simulation cell was constructed, and the TiO<sub>2</sub> nanoparticle positioned at lattice points associated with the primitive cubic Bravais lattice. Two of the dimensions of the simulation cell were reduced such that the nanoparticle agglomerated with its periodic neighbours in two dimensions under MD simulation facilitating the sheet. NVT simulation was then performed at 2000 K for 3.5 ns to facilitate crystallisation of the nanosheet. Periodic boundary conditions were imposed to facilitate replication of the structure of the nanosheet in two-dimensions. The low-temperature structural model was then generated by cooling the system to 0 K under NVT MD simulation until the configurational energy converged.

**Nanoporous Architecture.** To capture the (cubic) symmetry of the nanoporous architecture, a simulation cell with cubic symmetry was constructed and a nanoparticle of TiO<sub>2</sub> was positioned at lattice points associated with the primitive cubic Bravais lattice. The size of the simulation cell was then reduced in all three dimensions to enable the nanoparticle to agglomerate in all three spacial directions. NVT simulation was then performed at 2000 K for 3.5 ns to facilitate crystallisation. Periodic boundary conditions were used to replicate the structure infinitely in three

dimensions. The low-temperature structural model was then generated by cooling the system to 0 K under NVT MD simulation until the configurational energy converged.

**Bulk.** A nanoparticle of  $\text{TiO}_2$  was positioned within a cubic simulation cell and pressure was imposed upon the system such that the ions comprising the molten nanoparticle filled the simulation cell completely. Specifically, NPT simulation was performed at 2000 K with a pressure of 15 GPa for 3.5 ns during which time the  $\text{TiO}_2$  crystallized. Analysis of the structure revealed domains of rutile, brookite and (similar to) baddeleyite - a high-pressure phase of  $\text{TiO}_2$  with 7-coordinate Ti. Accordingly, the pressure was released and the material was annealed under NPT simulation at 2000 K for 10 ns during which time the domains of baddeleyite annealed out leaving rutile and brookite phases.

The procedures for generating atomistic models for nanomaterials are described in more detail in refs [12]. The final, low-temperature nanostructures are shown in fig. 2.

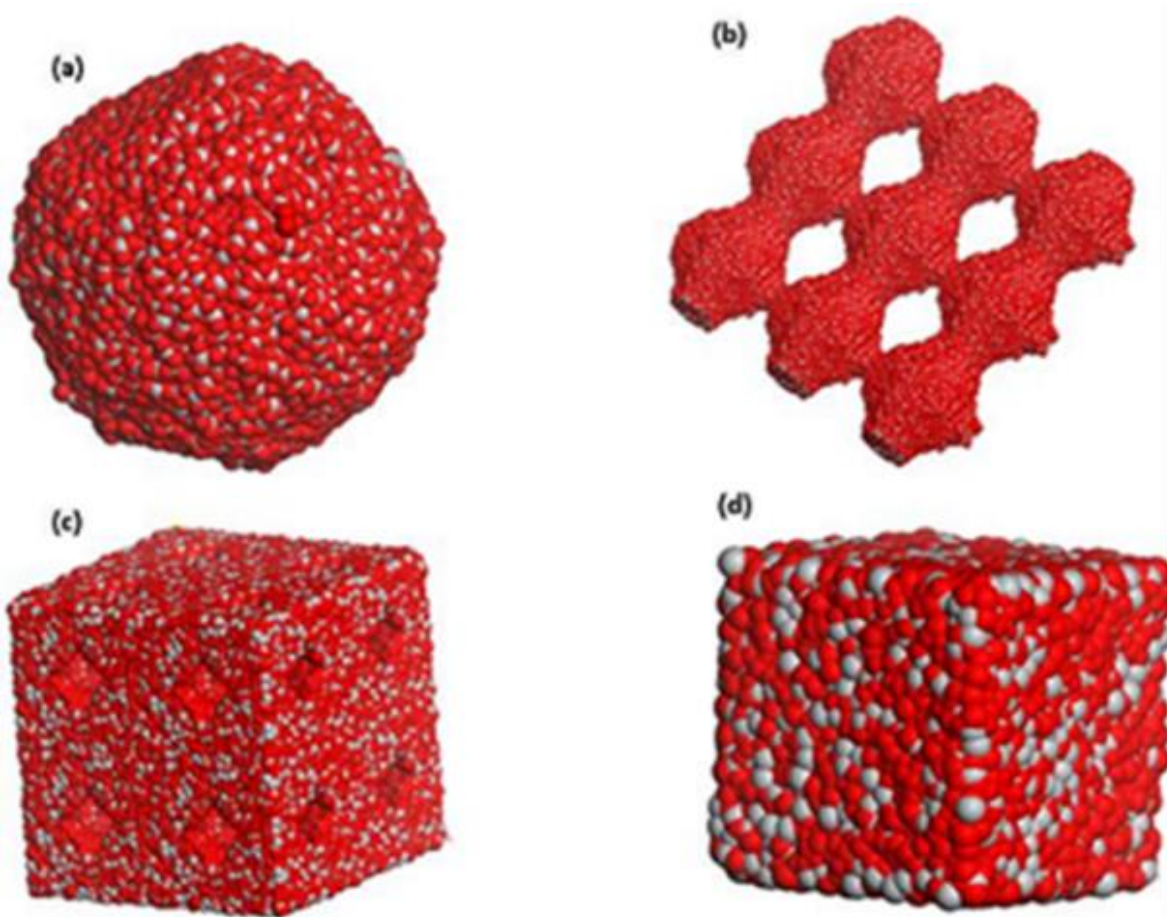


**Figure 2.** Atomistic models for the  $\text{TiO}_2$  nanostructures. (a) Nanosphere, (b) nanosheet, (c) nanoporous architecture and (d) bulk.

## Crystallisation

Crystallisation is evidenced by the change in the configuration energies as a function of time, and is shown in, figure 3. At the start of the simulation the configuration energies are high (indicative of the amorphous structure) and then a nucleating seed spontaneously evolves and nucleates the crystallisation of the nanomaterial. During crystallisation the configurational energy reduces until it reaches a plateau after the nanostructure has fully crystallised.

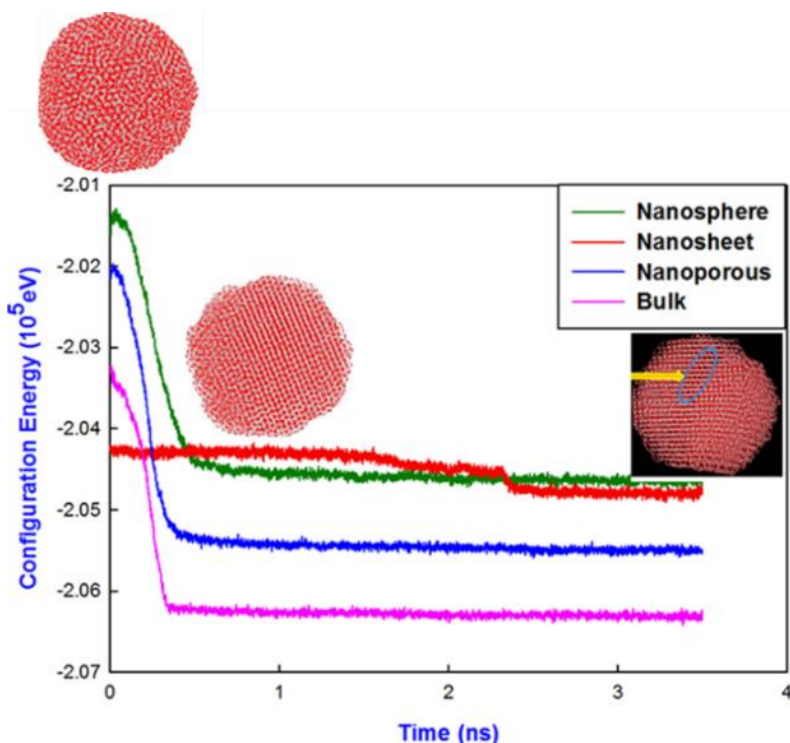


**Figure 3.** Configuration energy, calculated as a function of time, for the  $\text{TiO}_2$  nanoparticle, nanosheet, nanoporous architecture and bulk. The atomistic structure of the nanoparticle is shown at various points during the crystallisation depicting the amorphous (top left) to crystalline (middle, right) transition.

The latent heat of crystallization is the difference in the configuration energy between the amorphous and the crystalline nanostructures and are calculated to be 53, 59 and 52  $\text{kJmol}^{-1}$  for the nanosphere, nanoporous and bulk architectures respectively. The values are in reasonable accord with experiment; the measured heat of fusion of rutile  $\text{TiO}_2$  is about 50  $\text{kJmol}^{-1}$ .<sup>[13]</sup> The structures of the amorphous, partially crystalline and fully crystalline structure of the  $\text{TiO}_2$  nanoparticle are shown inset in fig. S2.

Contrary to other nano-architectures, the nanosheet crystallized during agglomeration of neighbouring nanospheres, under the NPT ensemble and therefore there is not a significant drop in the configuration energy as a function of time, fig. 3. This is firstly evidenced by the corresponding configuration energy vs time curve remaining near constant from 0 to 1.5 ns followed by a slight drop of energy from 1.5 to 2.25 ns. Above 2.25 ns there is a sudden reduction of energy, amounting to 5  $\text{kJ}\cdot\text{mol}^{-1}$ , which though noticeable, is not as large as the latent heat of crystallisation associated with nucleation to crystallisation transition. Such change can be ascribed to annealing (Oswald ripening) of a grain boundary.

## RESULTS

Analysis of the model nanostructures, using molecular graphics and calculated radial distribution functions (not shown), reveals that the  $\text{TiO}_2$  crystallises into the rutile and brookite polymorphic crystal structures. The atomistic models were then analysed further, to better understand the structure of the entrance sites associated with Li intercalation/deintercalation.

### **Mesoporous $\text{TiO}_2$**

The model of mesoporous  $\text{TiO}_2$  is shown in fig 4. In particular, fig 4(a) shows an HRTEM image of the real material [3], which can be compared to the atomistic model in fig 4(b); the positions of possible entrance sites for Li intercalation are highlighted by the yellow arrows in each figure. Polyhedral rendering of the structure ( $\text{TiO}_6$  polyhedra) is shown in fig 4(c), which reveals more clearly the 1x1 tunnels in which the Li ions intercalate and reside.  $\text{TiO}_6$  octahedra in the plane of the page are blue and  $\text{TiO}_6$  octahedra below the plane of the page are white. Accordingly, in the plane of the page, there are vacant 1x1 tunnels above the white  $\text{TiO}_6$  polyhedra into which the Li ions intercalate and reside.

It is difficult to appreciate the entrance sites with these two-dimensional images of the structure and therefore Connolly surfaces were calculated to reveal the accessible surface. The image in fig 4(d) shows the Connolly surface and enables a perspective view of the surface of the internal pore. An enlarged segment of the pore is shown in fig 4(e), which reveals the entrance sites for Li intercalation into the 1x1 tunnels; a ball and stick model of the atom positions is shown inset in fig 4(e) to illustrate how the individual atoms facilitate the structure of the entrance sites. Li ions are shown entering the 1x1 tunnels for illustration. The images of the mesoporous  $\text{TiO}_2$  depict atom positions comprising the model – no images are schematic.

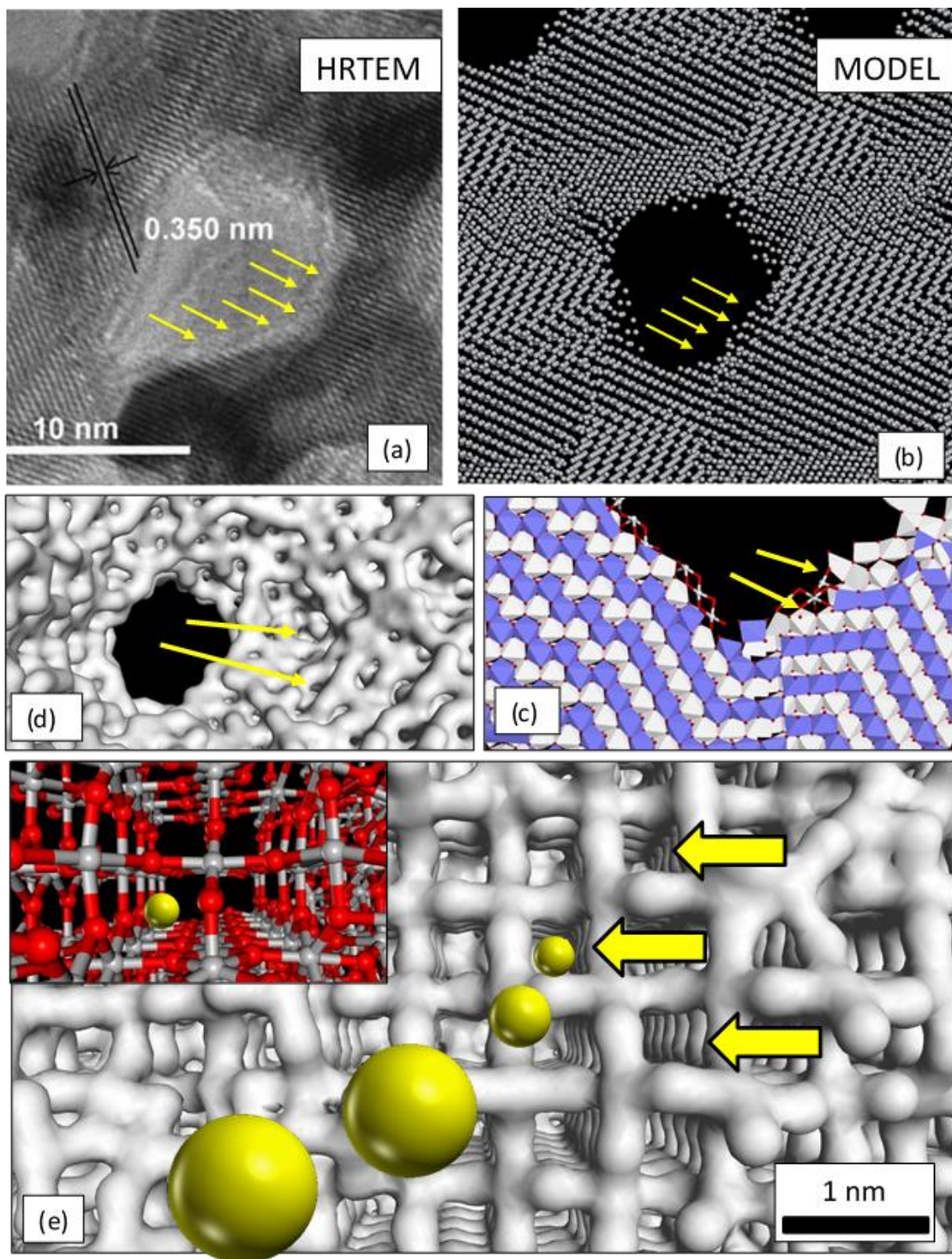


**Figure 4.** Atomistic structure of nanoporous  $\text{TiO}_2$ . (a) HRTEM image from ref [3]. (b) Sphere model representation of the atom positions comprising the atomistic model (only Ti shown). (c) Polyhedral rendering of the  $\text{TiO}_6$  octahedra showing the 1x1 tunnels. (d) Connolly surface rendered model looking along one of the pores of the nanomaterial. (e) Connolly surface showing the entrance sites to the 1x1 tunnels; a ball and stick model is shown inset (Ti is grey and oxygen is red).

## TiO<sub>2</sub> nanosheet

The atomistic model of the TiO<sub>2</sub> nanosheet is shown in fig 5. Fig 5(a,b) show the atom positions. It is difficult to appreciate the structure of the entrance sites via inspection of the atom positions, fig 5(a,b). Conversely, visualisation of the accessible surface, via calculated Connolly surface, provides insightful information, fig 5(c). A segment of (c) is shown enlarged in (d) and (e) using polyhedral and Connolly surface rendering respectively to reveal more clearly the accessible surface entrance sites.

Close inspection of fig 5(e) reveals many entrance sites with square profile. In particular, the 1x1 tunnels highlighted in the green circle, show (visually) that the entrance sites are large enough for Li to intercalate. However, as the surface of the nanosheet curves, the size and shape of other entrance sites change (red circle) preventing Li intercalation. Indeed, some entrance sites are blocked.

In the perfect bulk material, the 1x1 tunnel size is 3.3x3.3Å (cross section). Analysis, of the entrance sites in the mesoporous model reveals that some of the entrance sites are much larger than this (4.2x4.5Å) and would likely facilitate facile intercalation. Conversely, others are much smaller (2.7x4.9Å), preventing intercalation. The sizes of the 1x1 tunnels, inside the mesoporous TiO<sub>2</sub>, also show considerable structural variation, which would impact upon the transport of Li inside the host lattice and storage capacity.

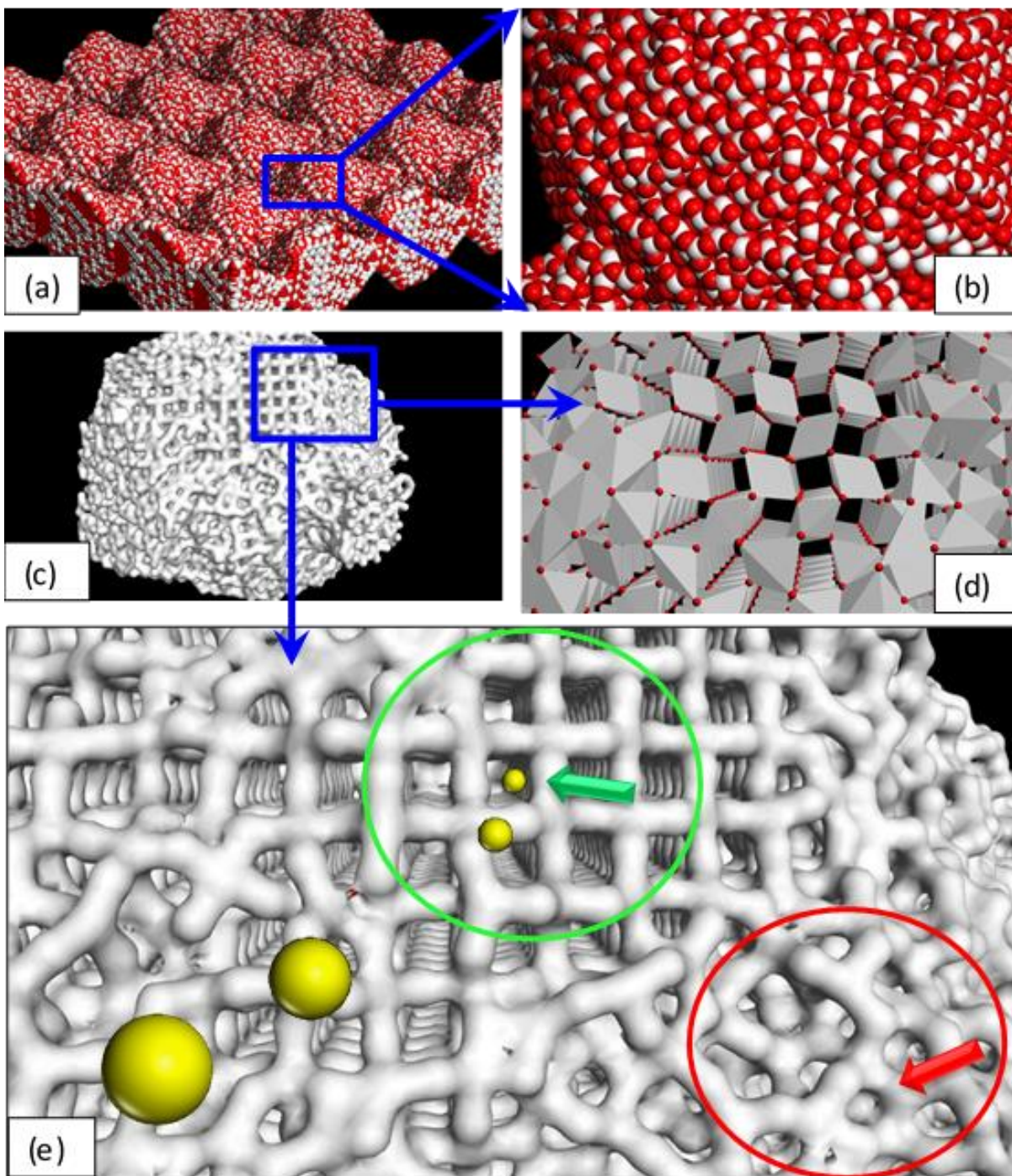


**Figure 5.** Atomistic structure of the TiO<sub>2</sub> nanosheet. (a) Sphere model representation of the atom positions; Ti is grey and oxygen is red. (b) Enlarged segment of (a). (c) Segment of the nanosheet, viewed perpendicular to the surface, revealing the atomistic structures of the surface entrances (Connolly surface rendered model). (d) Polyhedral rendered model of an enlarged segment of (c). (e) Enlarged segment of (c); Li (yellow) is superimposed on the atomistic model illustrating (as a schematic) the intercalation of Li into the surface and residing in one of the 1x1 tunnels. The region highlighted in green shows viable surface entrance sites. Conversely, the region highlighted in red, shows a considerable change in surface entrance site structure, which would likely impede Li intercalation.

## TiO<sub>2</sub> Nanoparticle

The atomistic model of the nanoparticle is shown in fig 6. The atom positions are shown in fig 6(a), which reveals some planar faceting of the surface occurs (top right corner of image). The curvature is therefore not smoothly continuous, which will influence the structure of the entrance sites. Similar to mesoporous and nanosheet models, entrance sites with square profile are observed, fig 6(c,d). Similarly, the curvature changes profoundly the structure of entrance sites, fig 6(e). The model structure of the nanoparticle is shown superimposed with a HRTEM image in fig 7; the close accord helps validate the model. [14]

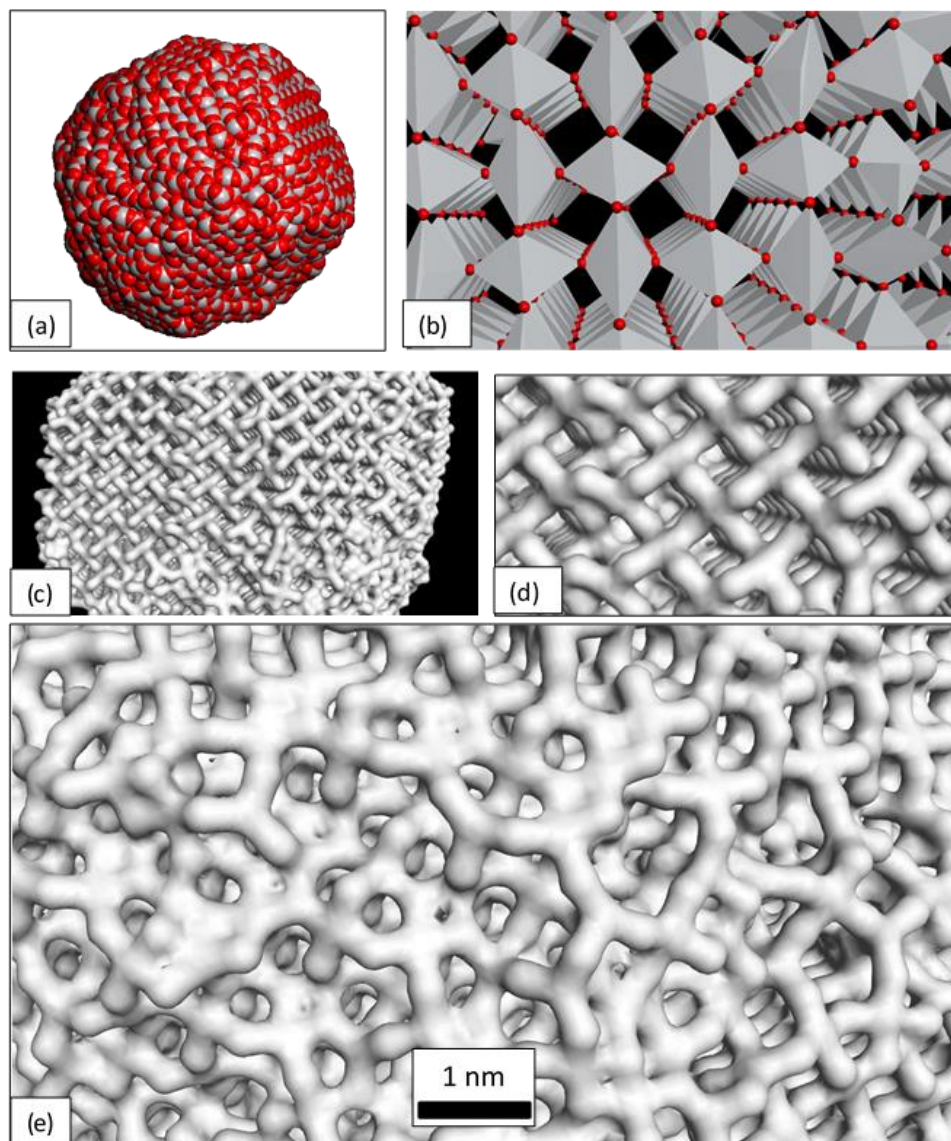


**Figure 6.** Atomistic structure of the TiO<sub>2</sub> nanoparticle. (a) Sphere model representation of the atom positions; Ti is grey and oxygen is red. (b) Polyhedral rendering of part of the surface of the nanoparticle showing the 1x1 tunnels (view looking perpendicular to the surface) which terminate at the surface. (c) (Connolly) surface rendered model of the nanoparticle (view is perpendicular to the surface) revealing the atomistic structures of the entrance sites to the 1x1 tunnels. (d) enlarged view of (c) showing more clearly the 1x1 tunnels. (e) View looking at a different region of the surface to show the considerable structural diversity of surface entrance sites.

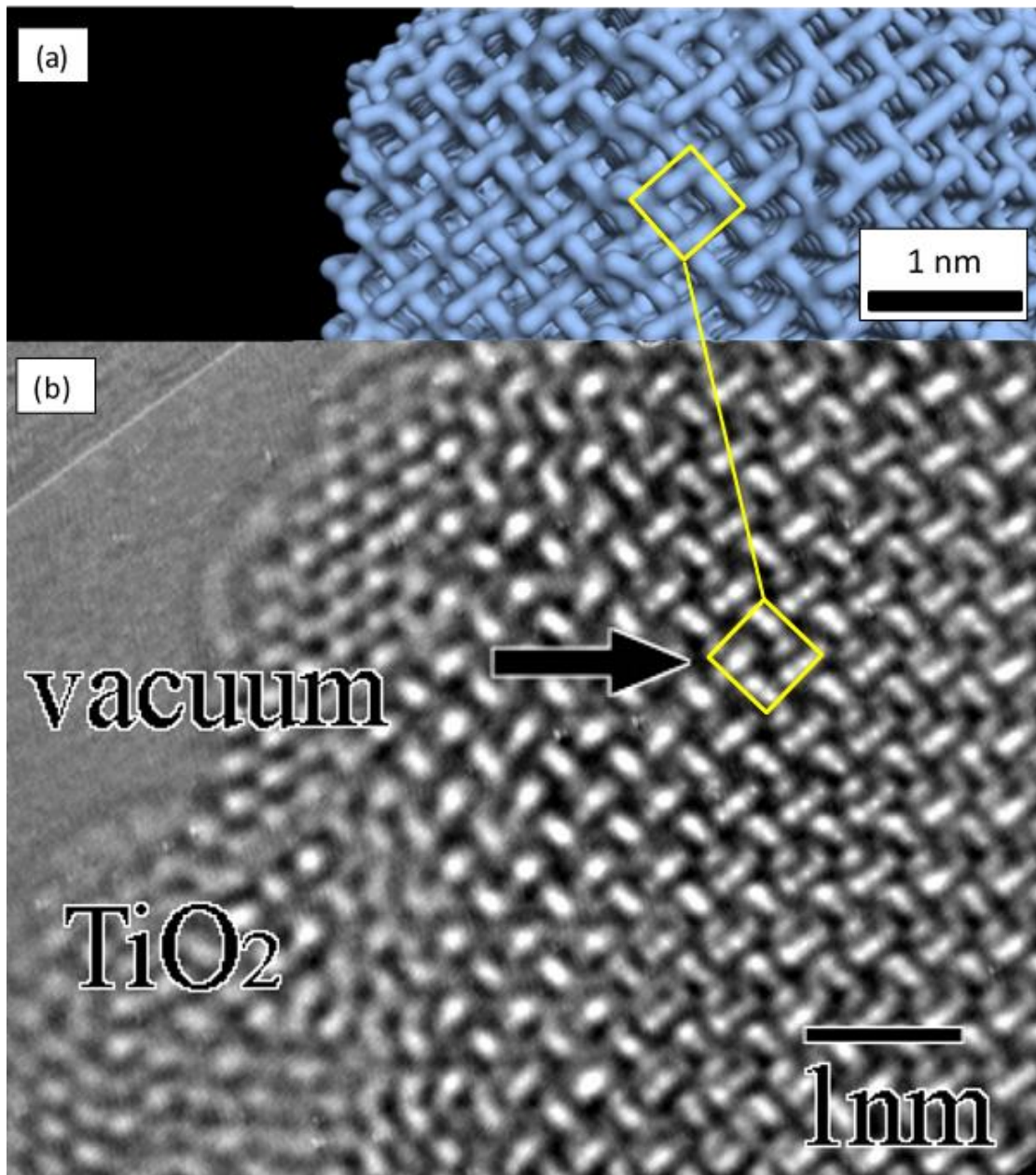


**Figure 7.** Nanostructured  $\text{TiO}_2$  model compared to experiment. (a) View looking perpendicular to the surface entrance of the atomistic model. (b) Spherical aberration corrected HRTEM reproduced with permission from Institution of Physics Publishing [14] A  $1 \times 1$  tunnel is highlighted in both the model (a) and real (b) material.

## X-Ray Diffraction (XRDs)

To further validate our structural models, XRD patterns, calculated for each of the model  $\text{TiO}_2$  nanostructures, are compared to experiment (brookite, rutile and  $\alpha\text{-PbO}_2$  structured  $\text{TiO}_2$ ) [15] in fig 8.

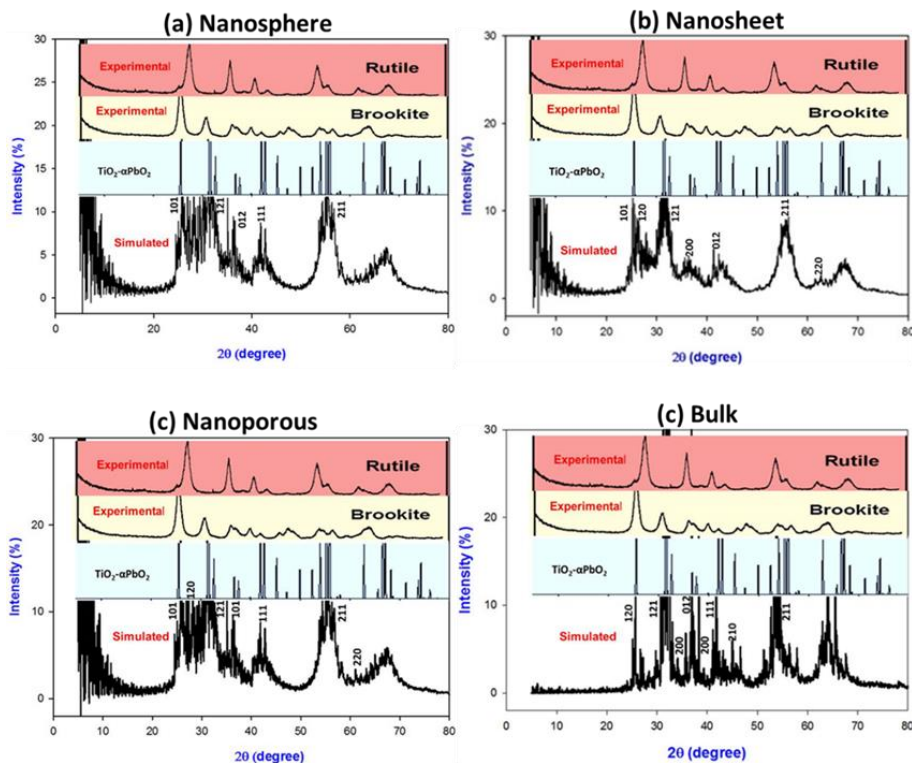


**Figure 8.** Calculated X-Ray Diffraction (XRD) patterns of the atomistic models of nanostructured  $\text{TiO}_2$  compared with experimental data (reproduced with permission of The Electrochemical Society ref [15]) for  $\text{TiO}_2$ ; brookite, rutile and  $\alpha\text{-PbO}_2$  polymorphs. We note that (d) shows the bulk structure prior to annealing out the baddeleyite polymorph.

Inspection of fig. 8, reveals evidence of the brookite polymorph in each of the nanostructures; peaks at 27, 33 and 37 ° can be indexed to brookite (120), (121) and (012) planes respectively. Similarly, the models also exhibit characteristics of rutile and  $\alpha\text{-PbO}_2$ -type phases. We note that the XRD trace for the bulk  $\text{TiO}_2$  is generally sharper compared to the nanomaterials. In particular, a greater accord with rutile and  $\alpha\text{-PbO}_2$ -type structure, rather than brookite, is evident.  $\text{TiO}_2$  nanocrystals comprising both brookite and rutile polymorphs have been reported [16]; the authors proposed that the relative proportions of such polymorphs can be varied facilitating tuneable photocatalytic properties of the nanomaterial.

## Microstructure

Once intercalated into the  $\text{TiO}_2$ , the Li ions need to move within the host lattice; typically, it is understood that Li ions move and reside within the  $1 \times 1$  tunnels. Accordingly, microstructural features, such as grain-boundaries, will impact considerably upon transport and storage within the host.<sup>[17, 18]</sup> Molecular graphics was used to explore the microstructural features comprising the nanoparticle, nanosheet, nanoporous architecture and bulk, fig. 9; the (perfect) crystal structures of the parent rutile, brookite and anatase polymorphs of  $\text{TiO}_2$  are shown in fig. 10 to compare.

Slices of each (model) nanomaterial were cleaved to reveal the connectivity of the  $\text{TiO}_6$  octahedra. Octahedra comprising the upper plane are coloured blue, and polyhedra comprising the lower plane are white. For the nanoparticle, fig 9(a), we observe large domains of rutile structured  $\text{TiO}_2$  together with microtwinning; smaller domains of brookite-structure  $\text{TiO}_2$  are also evident. For the nanosheet, fig 9(b), we observe an even mix of domains conforming to brookite and rutile polymorphs. Similarly, the nanoporous model, fig 9(c), comprises an even mix of brookite and rutile. We note that the domain-boundaries are normally coherent between the brookite and rutile polymorphs. The bulk material, fig 9(d,e) also comprises both rutile and brookite, but there is also a grain-boundary that traverses the slice, fig 9(d). An alternative view of the model reveals a structure similar to the baddeleyite polymorph, fig 9(e). We note that the bulk model, depicted in fig 9(d,e), is under 10 GPa pressure; upon release of the pressure, the baddeleyite polymorph transforms structurally to leave only the brookite and rutile polymorphs. Inspection of the atomistic models of all nanostructures also reveals a variety of grain-boundaries/dislocations and point defects (predominantly vacancies). Nanostructured  $\text{TiO}_2$  comprising mixed polymorphic phases have been reported<sup>[19, 20]</sup>.

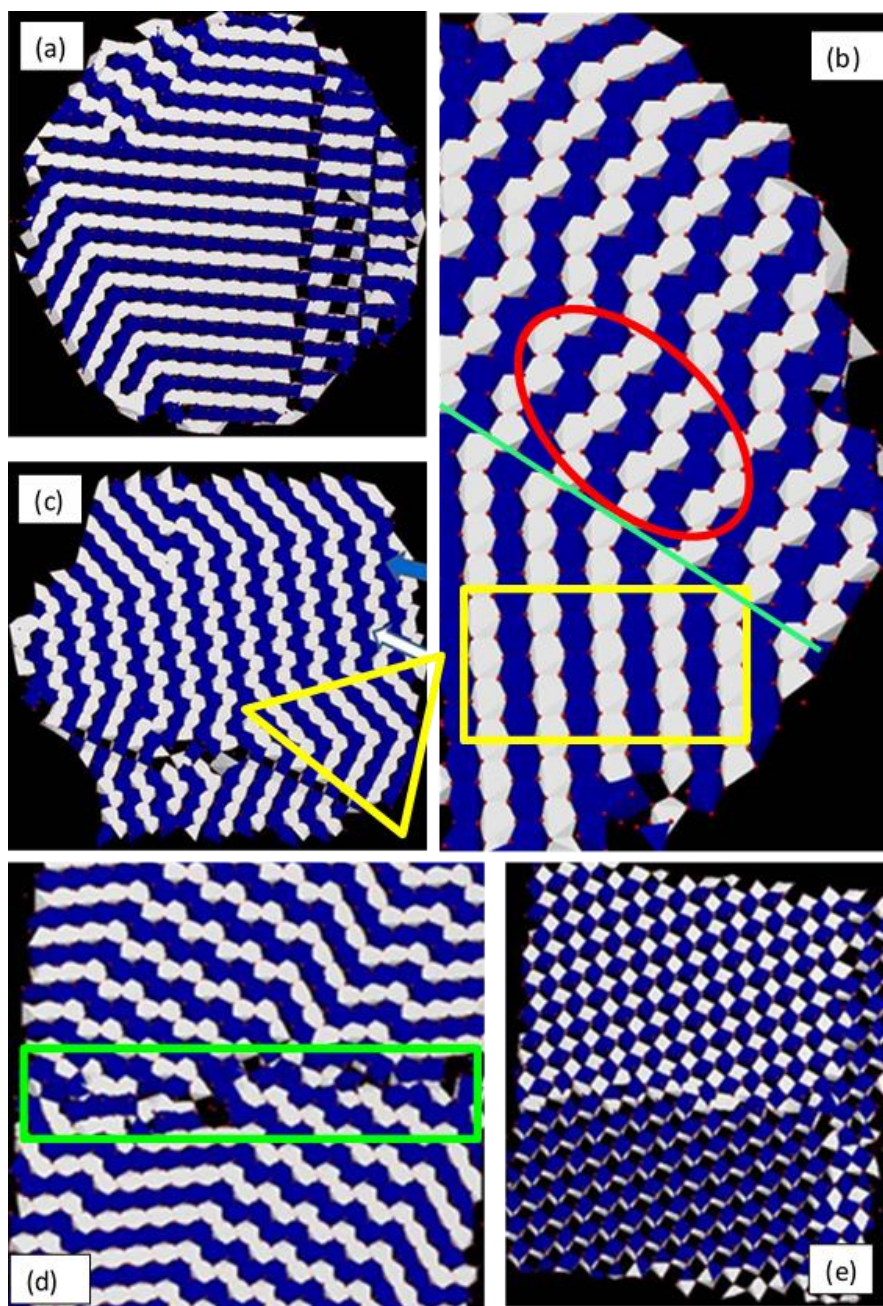


**Figure 9.** Microstructural features comprising the  $\text{TiO}_2$  nanostructures. (a)  $\text{TiO}_2$  nanoparticle (b) nanosheet - rutile and brookite domains designated by yellow and red regions respectively; the green line is a junction or domain boundary, (c) nanoporous architecture, (d,e) bulk. Polyhedral rendering of the  $\text{TiO}_6$  octahedra was used to depict the  $1 \times 1$  tunnels more clearly. The region enclosed by the red oval and yellow rectangle (b) correspond to the brookite and rutile polymorphs respectively; the yellow triangle in (c) reveals microtwinning of the rutile structure; the green rectangle reveals a grain-boundary/dislocation which comprises point defects. We note that (d,e) shows the bulk structure prior to annealing out the baddeleyite polymorph.

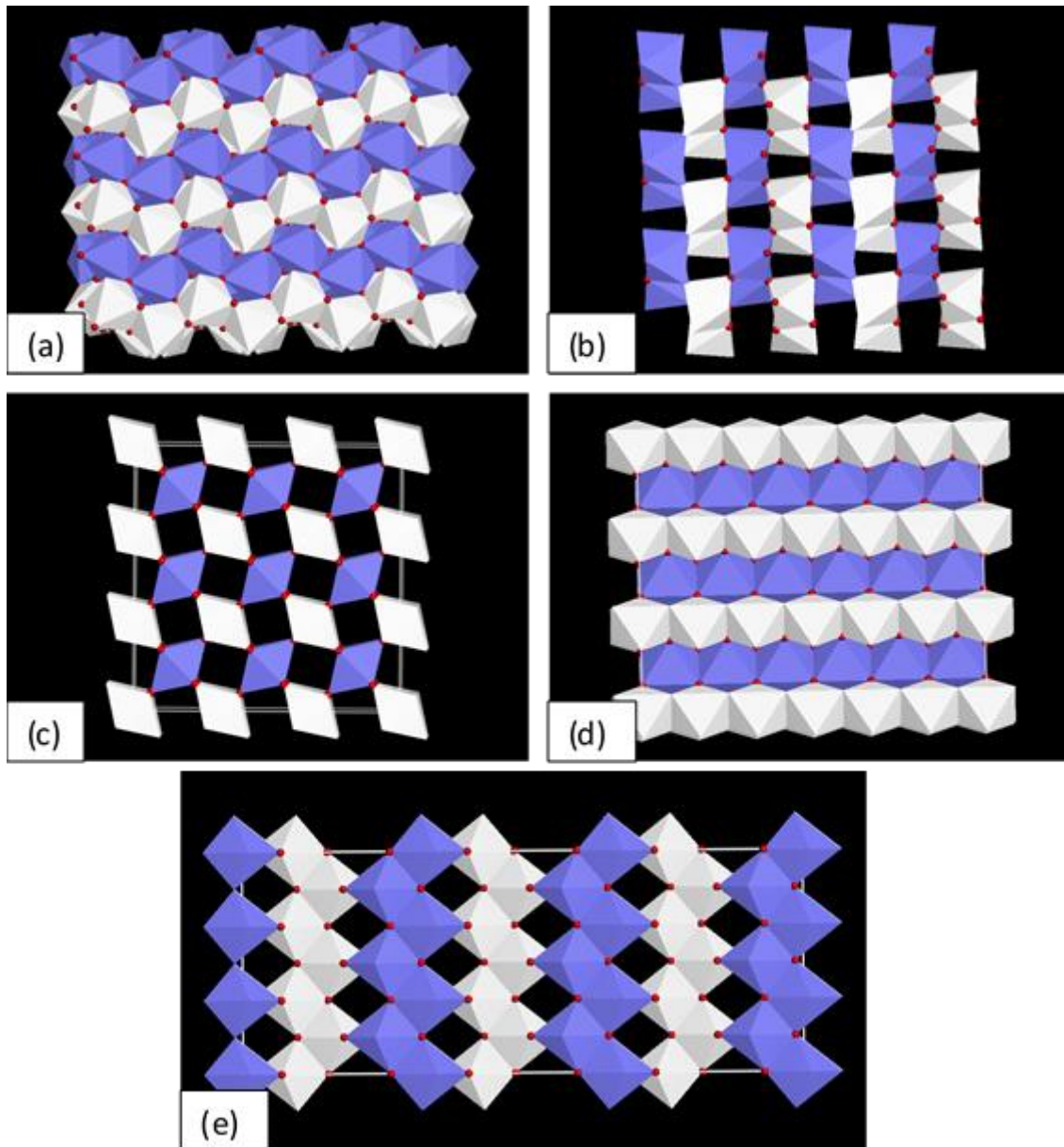


**Figure 10.** Polymorphic crystal structures of brookite (a,b), rutile (c,d) and anatase (e), showing the zig-zag (brookite) and straight (rutile) 1x1 tunnels. Views depict: (a) brookite [100]; (b) brookite [001]; (c) rutile [001]; (d) rutile [100]; (e) anatase [100].

## DISCUSSION

Central to the viability of a nanomaterial acting as an electrode for a Li-ion battery are the kinetics associated with Li intercalation and transport within the host nanomaterial. Atomistic simulation can be used to predict the kinetics associated with the intercalation of Li into the host lattice by calculating the activation energy barrier for Li to pass through the surface of the host. Indeed, Tompsett et al. calculated the energy associated with Li insertion into the  $\beta$ -MnO<sub>2</sub> (101) surface to be >0.6 eV; the (101) surface dominates the equilibrium morphology. Li mobility within the bulk was calculated to be 0.17eV and therefore Li intercalation is predicted to be the rate limiting step [7]. The authors also argue that nanostructuring might help reduce the (high) energy barrier to Li intercalation. Characterisation of the atomistic structure of the surface sites is therefore a first step in exploring the energetics of Li intercalation and a pre-cursor to being able to modify the surface structures to facilitate energetically facile intercalation/deintercalation and hence increase the power of Li-ion devices.

Here, we show that the structure of the surface entrance sites for nanostructured TiO<sub>2</sub> deviate considerably compared to the parent (bulk) material, which will influence the energetics and hence kinetics associated with Li intercalation. Our simulations reveal that the structures of the entrance sites for Li intercalation are critically dependent upon the curvature of the surfaces. We predict therefore that nanostructuring can be used to tune the power of a battery. Changes may include, for example, the nanoparticle radius, mesoporous wall thickness and architecture. Similarly, the architecture of the mesoporous TiO<sub>2</sub> can be changed by using alternative silica templates during synthesis. In particular, the architecture of the real material, fig 1(b), conforms to the Ia3d space symmetry [3]. Alternative silica templates, with different sizes, shapes and pore connectivities can be used to facilitate nanostructuring of the TiO<sub>2</sub>.

### Li transport numbers

In addition to the activation energy barrier, the power of a Li-ion battery is directly correlated with the Li-ion transport number. Specifically, the number of Li ions that can be intercalated/deintercalated into the host lattice as a function of time. The transport number will depend upon the number of viable surface entrance sites per unit area. In particular, fig 5(e), shows regions on the surface of the TiO<sub>2</sub> nanoparticle that facilitate Li intercalation (green oval) and conversely regions where the surface entrance sites are too small to facilitate intercalation (red oval). We also note that some regions on the surface are blocked towards Li intercalation, which emanate as a consequence of the crystallographic direction with respect to the nanostructure. The atomistic models therefore proffer some insight into the Li ion transport numbers as limited by the concentration of viable entrance sites.

Experimentally, atom positions (coordinates), measured using, for example, XRD, provide a quantitative depiction of structure. However, for mesoporous materials, where the unit cells comprise tens of thousands of atoms, the atom positions are no longer intuitive; rather HRTEM images, fig 4(a), manifest as *quantitative* and accessible depictions of structure. Similarly, a list of the atom coordinates comprising an atomistic model are quantitative depictions of structure, which can be presented in an accessible fashion using molecular graphics. All the images presented here are representations of the actual atom positions (no images are schematic). Accordingly, we argue that the (molecular graphical) images manifest as a quantitative depiction of structure.

Previously, we showed that atomistic models of nanomaterials, generated by ‘simulating synthesis’, are in quantitative structural accord with experiment [21]. In this present study, our images of nanostructured TiO<sub>2</sub> are in close accord with experiment – fig 4(a,b) and fig 7(a,b) . The close comparison with HRTEM acts as a validation of the model. In particular, if we can generate atomistic structures in accord with experiment, by simulating the

crystallisation<sup>ii</sup>, we can have confidence that the structural complexity of the model reflects the real material. Moreover, we can be assured that the information derived from using the model is reliable. In particular, at present, experiment (HRTEM) cannot resolve the structure of the entrance sites, which are central to the speed of Li intercalation and hence battery power. Here, we show the rich variety of atomistic structures and sizes of the entrance sites. Indeed, it might be assumed that the entrance sites are structurally similar, this study reveals that they are profoundly different.

## CONCLUSION

Molecular dynamics simulation has been used to generate atomistic models of nanostructured TiO<sub>2</sub> including: nanoparticles, nanosheets and mesoporous architectures. The hierarchical structural complexity of the system was captured within the model by ‘simulating synthesis’. Specifically, we simulated crystallisation of the system starting from amorphous precursors – the only variable used to direct the evolution of the nanostructures was the temperature of crystallisation. The resulting models reveal the structures of the entrance sites, which facilitate Li intercalation. The structures of the entrance sites show considerable structural variation, spanning large ‘diameter’ entrances sites, which would likely facilitate facile Li intercalation to small diameter entrance sites, which would make Li intercalation difficult. The structural variation is critically dependent upon the nanostructuring – specifically the curvature of the surfaces, which emanate from the radius of the nanoparticle and architecture of the mesoporous system.

## AUTHOR INFORMATION

Corresponding Author

\*phuti.ngoepe@ul.ac.za

Notes

The authors declare no competing financial interest

## ACKNOWLEDGEMENTS

This work is supported by the South African Research Chair Initiative of the Department of Science and Technology and National Research Foundation, Pretoria, the Department of Science and Technology HySA Lithium Ion Batteries and Supercapacitors Project, Pretoria and the Centre for High Performance Computing (CHPC) in South Africa.

---

<sup>ii</sup> With temperature being the only variable that can be used to influence the structural evolution

## REFERENCES

- <sup>1</sup> Armand, M.; Tarascon, J. -M.  
Building better batteries  
*Nature* 451, **2008**, 652-657.
- <sup>2</sup> Choi, N. S.; Chen, Z. H.; Freunberger, S. A.; Ji, X. L.; Sun, Y. K.; Amine, K.; Yushin, G.; Nazar, L. F.; Cho, J. and Bruce, P. G.  
Challenges Facing Lithium Batteries and Electrical Double-Layer Capacitors  
*Angew. Chem. Int. Ed.* 51, **2012**, 9994 – 10024
- <sup>3</sup> Ren, Y.; Hardwick, L. J.; Bruce, P. G. Lithium Intercalation into Mesoporous Anatase with an Ordered 3D Pore Structure. *Angew. Chem. Int. Ed.* **2010**, 49, 2570 - 2574.
- <sup>4</sup> Jiao, F.; Bruce, P. G. Mesoporous Crystalline  $\text{-MnO}_2\text{-}$  a Reversible Positive Electrode for Rechargeable Lithium Batteries. *Adv. Mater.* **2007**, 19, 657 - 660.
- <sup>5</sup> Uchaker, E. and Cao, G.  
Mesocrystals as electrode materials for lithium-ion batteries  
*Nano Today* 9, **2014**, 499-524
- <sup>6</sup> Sayle, T. X. T.; Kgatwane, K.; Ngoepe, P. E. and Sayle, D. C.  
'Breathing-crystals' the origin of electrochemical activity of mesoporous Li-MnO<sub>2</sub>  
*J. Mater. Chem. A*, 4, **2016**, 6456–6464
- <sup>7</sup> Tompsett, D. A.; Parker, S. C.; Bruce, P. G; Islam, M. S.  
Nanostructuring of  $\beta\text{-MnO}_2$ : The Important Role of Surface to Bulk Ion Migration.  
*Chem. Mater.* 25, **2013**, 536 - 541.
- <sup>8</sup> Zheng, X.; Kuang, Q.; Yan, K.; Qiu, Y.; Qiu, J. and Yang, S.  
Mesoporous TiO<sub>2</sub> Single Crystals: Facile Shape-, Size-, and Phase-Controlled Growth and Efficient Photocatalytic Performance  
*ACS Appl. Mater. Interfaces*, 5, **2013**, 11249–11257
- <sup>9</sup> Matsui, M.; Akaogi, M.  
Molecular dynamics simulation of the structural and physical properties of the four polymorphs of TiO<sub>2</sub>.  
*Mol. Simul.* **1990**, 239 - 244.
- <sup>10</sup> Sayle, D. C. and Sayle, T. X. T.  
High-Pressure Crystallisation of TiO<sub>2</sub> Nanocrystals  
*J. Comput. Theo. Nanos.* 4, **2007**, 299 - 308.
- <sup>11</sup> Smith, W.; Forster, T. R. <http://www.dl.ac.uk/TCSC/Software/DLPOLY>.
- <sup>12</sup> Sayle, D. C.; Seal, S.; Wang, Z. W.; Mangili, B. C.; Price, D. W.; Karakoti, A. S.; Kuchibhatla, S. V. T. N.; Hao, Q.; Möbus, G.; Xu, X. and Sayle, T. X.T.  
Mapping Nanostructure: A Systematic Enumeration of Nanomaterials by Assembling Nanobuilding Blocks at Crystallographic Positions  
*ACS Nano*, 2, **2008**, 1237–1251
- <sup>13</sup> Weast, R. C. (Editor)  
*Handbook of Chemistry and Physics*, 55<sup>th</sup> edition, 1974-1975 CRC Press Inc. ISBN 087819-451-1
- <sup>14</sup> Yoshida, K.; Kawai, T.; Nambara, T.; Tanemura, S.; Saitoh, K.; Tanaka, N.  
Direct observation of oxygen atoms in rutile titanium dioxide by spherical aberration corrected high-resolution transmission electron microscopy.  
*Nanotechnology* 17, **2006**, 3944 - 3950.
- <sup>15</sup> Dambournet, D.; Belharouak, I. and Amine, K.  
Nanosized TiO<sub>2</sub> anatase, rutile and brookite anodes for Li-ion batteries.  
*Electrochem. Soc.*, 2009. 215th ECS Meeting, Abstract #445, © The Electrochemical Society
- <sup>16</sup> Xu, H. and Zhang, L.  
Controllable one-pot synthesis and enhanced photocatalytic activity of mixed-phase TiO<sub>2</sub> Nanocrystals with tunable brookite/rutile ratios.  
*J. Phys. Chem. C* 113, **2009**, 1785 - 1790.
- <sup>17</sup> Dawson, J. A. and Tanaka, I.

---

Li Intercalation into a  $\beta$ -MnO<sub>2</sub> Grain Boundary

ACS Appl. Mater. Interfaces 7, **2015**, 8125–8131

<sup>18</sup> Kerisit, S.; Chaka, A. M.; Droubay, T. C. and Ilton, E. S.

Shell Model for Atomistic Simulation of Lithium Diffusion in Mixed Mn/Ti Oxides

J. Phys. Chem. C 118, **2014**, 24231–24239

<sup>19</sup> Zhao, W. N.; Zhu, S. C.; Li, Y. F. and Liu Z. P.

Three-phase junction for modulating electron–hole migration in anatase–rutile photocatalysts

Chem. Sci., 6, **2015**, 3483–3494

<sup>20</sup> Shang, C.; Zhao, W. N. and Liu, Z. P.

Searching for new TiO<sub>2</sub> crystal phases with better photoactivity

J. Phys.: Condens. Matter 27, **2015**, 134203

<sup>21</sup> Sayle, T. X. T.; Molinari, M.; Das, S.; Bhatta, U.; Möbus, G.; Parker, S. C. Seal, S. and Sayle, D. C.

Environment-mediated structure, surface redox activity and reactivity of ceria nanoparticles

Nanoscale 5, **2013**, 6063–6073